Fibroblast Growth Factor 5 (FGF5) and Its Missense Mutant FGF5-Y174H Underlying Trichomegaly: A Molecular Dynamics Simulation Investigation

Skyler H. Hoang[1]

[1]Department of Cell Biology and Neuroscience Rutgers University, Piscataway, New Jersey, 08854, USA

Email: hung.hoang@rutgers.edu

Abstract

The missense mutation Y174H of FGF5 (FGF5-Y174H) had been associated with trichomegaly, characterized by abnormally long and pigmented eyelashes. The amino acid tyrosine (Tyr/Y) is conserved across many species, proposedly holding important characteristics for the functions of FGF5. One-microsecond molecular dynamics simulations along with protein-protein docking and residue interacting network analysis were employed to investigate the structural dynamics and binding mode of both wild-type (FGF5-WT) and its mutated counterpart (FGF5-Y174H). It was found that the mutation caused decreases in number of hydrogen bonds within the protein, sheet secondary structure, interaction of residues 174 with others, and number of salt-bridges. On the other hand, the mutation showed increases in solvent accessible surface area, number of hydrogen bonds between the protein and solvent, coil secondary structure, protein C-alpha backbone root mean square deviation, protein residue root mean square fluctuations, as well as occupied conformational space. In addition, protein-protein docking demonstrated that the mutated variant showed stronger binding affinity towards fibroblast growth factor receptor 1 (FGFR1). However, residue interacting network analysis demonstrated that the binding mode was drastically different from that of the FGF5-WT-FGFR1 complex. In conclusion, the mutation conferred more instability, stronger binding affinity towards FGFR1 with alteration in binding mode. These findings might help explain the decreased activation of FGFR1, underlying trichomegaly.

Introduction

Fibroblast growth factor (FGF) 5 (FGF5), belonging to the canonical FGF family as well as FGF4 subfamily, has a substantial impact on the regulation of cell differentiation and proliferation (Ornitz & Itoh, 2015). Particularly, FGF5 is most notable for its function in the regulation hair growth: by activating the fibroblast growth factor receptor 1 (FGFR1) and being predominantly produced in hair follicles, it acts as an inhibitor of hair elongation by promoting the transition from the hair follicle's growth phase, anagen, into the apoptosis-induced regression phase, catagen (Higgins et al., 2014). Simply put, it is required for the proper regulation of the hair development cycle. In terms of direct application, CRISPR/Cas9-mediated loss of FGF5 function promotes the production of longer wool in Chinese merino sheep, representing a valuable target for the wool industry (Li et al., 2017).

Other *in vitro*, *in vivo*, and clinical studies have demonstrated other functions of FGF5. In terms of molecular signaling, the FGF-FGFR signaling motif frequently depends on the phosphoinositide-3-kinase–protein kinase B/Akt (PI3K-AKT), rat sarcoma mitogen-activated protein kinase (RAS-MAPK), and signal transducer and activator of transcription (STAT) pathways, master regulators of many biological processes (Ornitz & Itoh, 2015). Particularly, in an *in vitro* cultured primary rat Schwann cells, FGF5 was demonstrated to be an autocrine regulator of Schwann cells that could regulate Schwann cell migration and adhesion through inhibiting extracellular signal-regulated protein kinases 1 and 2 (ERK1/2) MAPK activity and the upregulation of N-cadherin (Chen et al., 2020). Additionally, in a study with *in vitro* and clinical combined approach, FGF5 was found to be overexpressed in osteosarcoma cell lines and clinical tissue samples and to promote osteosarcoma cell proliferation by activating the MAPK signaling pathway, suggesting that FGF5 could be a therapeutic target for osteosarcoma (Han et al., 2019). On the other hand, in a study with *in vitro* and *in vivo* combined approach, FGF5 can contribute to the malignant progression of human astrocytic brain tumors by stimulating proliferation, migration, and tube formation in human umbilical vein endothelial cells via autocrine and paracrine effects (Allerstorfer et al., 2008). Additionally, an *in vitro* study showed that methylated exogenous FGF5 overexpression conferred

resistance to cisplatin treatment; meanwhile, FGF5 was not expressed in non-cancerous esophageal tissues, and only a small percentage of cells had it methylated, indicating that FGF5 methylation could be a sensitivity marker of esophageal squamous cell carcinoma to definitive chemoradiotherapy a biomarker (Iwabu et al., 2019). From a clinical perspective, a recent clinical study demonstrated that FGF5 may regulate to blood pressure, as patients with primary hypertension had abnormally high levels of FGF5 mRNA and protein expression, along with genetic variations that were related to their blood pressure (Ren et al., 2018). In conjunction, another clinical found concluded that the genetic variant rs148038 near FGF5 gene, highly present in the Filipino population, was strongly associated with blood pressure response to calcium channels blockers (Punzalan et al., 2022). A case-control association analysis found that the FGF5 polymorphism rs16998073 significantly increases the risk of preeclampsia in the Chinese Han population, suggesting that FGF5 may play a role in the progression of the disease (Xin et al., 2022). Overall, emerging explorations into the functions of FGF5 emphasizes the need for further research into this unique protein.

Recent evidence suggested that Y174 is an amino acid residue that is highly conserved across species, indicating critical roles in structure formation and functions of FGF5 and that the missense mutation Y174H may be a potential cause of trichomegaly, a disorder characterized by excessively long, pigmented, and thick eyelashes (Higgins et al., 2014; Rossetto et al., 2013). Y174 is characterized by its hydrophobic aromatic function group, whereas H174 is characterized by a positively charged imidazole functional group. This poses a question: will such a drastic difference interfere with structures and functions of FGF5? Herein, *in silico* approaches (i.e., molecular dynamics simulations and protein-protein docking) were used to test the hypothesis that the missense mutation could lead to severe conformational changes and protein instability, resulting in reduced binding at FGFR1 and the development of trichomegaly.

Method

1. Protein Retrieval and *in silico* mutagenesis

The structure of FGF5 was retrieved from AlphaFold Protein Structure Database (https://alphafold.ebi.ac.uk/), with accession number: P12034. PyMol 2.5 (https://pymol.org/2/) was used to perform the mutagenesis at 174 from tyrosine (Y174) to histidine (H174); the conformation with the least steric strain was applied. Ramachandran Plot Server (https://zlab.umassmed.edu/bu/rama/) was employed to validate the models; both showed 139 (97.015%) highly preferred and 4 (2.985%) preferred observations with no questionable observation (**Figure 1**)

2. Molecular Dynamics Simulation setup

YASARA Dynamics (Version 21.8.27) (Land & Humble, 2018) was used to construct macro-second molecular dynamics simulations with 1,001 snapshots of simulations each. The script md_run.mcr was applied towards the simulations of FGF5-WT and FGF5-Y174H. Simulation runs were optimized with: (1) steepest descent minimization without electrostatics (2) simulated annealing minimization of the solvent (3) simulated annealing of the solvent to adapt to deleted waters (4) running 50 steps of solvent MD (5) running local steepest descent minimization without electrostatics to remove bumps. Timestep settings were set at the followings: 1.25 femtosecond of intramolecular force substep and intermolecular forces are calculated for every 2.5 femtosecond. Concentration of NaCl was set at 0.9%; pH was set at 7.4. Pressure control was in Solvent Probe mode. Extension of the simulation cell is 20 Å larger than the protein. Shape of the simulation cell is cube. Forcefield used was AMBER14. Simulations were performed with long-range Coulombe forces (particle-mesh Ewald). “CorrectDrift” mode

was turned on to keep solute from diffusing around and crossing the periodic boundaries. Afterwards, md_analyze.mcr script was used to retrieve data for (1) solvent accessible surface area (SASA), (2) percentages of types of secondary structures throughout the simulations, (3) interactions between residue 174 and others, (4) root mean square deviation (RMSD) of C-alpha carbons of the proteins, (5) number of salt-bridges created by Lysine (Lys)/Arginine (Arg) and Aspartic acid (Asp)/Glutamic acid (Glu), protein residue root mean square fluctuations (RMSF).

3. Construction of PCA plot

The YASARA molecular dynamics simulation trajectory .sim files were then converted to GROMACS simulation .xtc files using md_convert.mcr script. The gmx_covar and gmx_anaeig functions in GROMACS 2022.4 were then used to retrieve principal component analysis (PCA) and eigenvalue data of the movement of C-alpha backbone of the proteins.

4. Protein-protein docking and constructing residue interacting network

Protein-protein docking was performed with HDock Server (Yan et al., 2017). The models with the highest scoring functions were used in this study. Prodigy Webserver (Xue et al., 2016) was then used to calculate the binding affinities at 25□. The protein-protein complexes were visualized with PyMol, and residue interactions analysis were created in the formed of network through Residue Interaction Network Server 3.0 (Clementel et al., 2022). Cytoscape 3.9.1 (https://cytoscape.org) was used to calculate degree, which counts for the number of edges or interactions a residue can form, for each respective residue. R (https://www.r-project.org) was used to create multiple-group histogram for the degree.

5. Visualization

Data visualization was accomplished with PyMol, GraphPad Prism 9 (https://www.graphpad.com/), YASARA, QtGrace (https://sourceforge.net/projects/qtgrace/), Cytoscape, R (with "ggplot2" package).

Results

1. The missense mutation Y174H alters interactions with the solvent

Parameters relevant to how proteins interact with its environment or solvent (solvent accessible surface are, number of hydrogen bonds within the protein, and between protein and solvent) were evaluated (**Figure 2**). Particularly, on average, FGF5-Y174H with 7178 ± 137.4 $Å^2$ showed higher solvent accessible surface area than FGF5-WT with 7346 ± 139.8 $Å^2$ (**Figure 2A**). FGF5-Y174 demonstrated apparent increase in solvent accessible surface area from approximately 200th ns to 300th ns and 700th ns to 1000th ns (**Figure 2A**). In addition, the number of hydrogen bonds within FGF5-Y174H was 96.59 ± 5.063, smaller than that of FGF5-WT with 97.31 ± 4.891 hydrogen bonds (**Figure 2B**). Specifically, the difference most apparent at 200th ns to 300th ns (**Figure 2B**). Alternatively, the number of hydrogen bonds within FGF5-Y174H was 251.6 ± 8.667, smaller than that of FGF5-WT with 255.7 ± 9.366 hydrogen bonds (**Figure 2C**). The difference is also most apparent at 200th ns to 300th ns (**Figure 2C**).

2. The missense mutation Y174H decreases sheet and increase coil secondary structures.

Parameters relevant to the secondary structures of (percentages of sheet, turn, and coil structures) were evaluated (**Figure 3**). Particularly, due to the mutation, the percentage of sheet structure weas decreased from 52.57% ± 3.270% to 49.78% ± 3.259% for FGF5-WT and FGF5-Y174H, respectively (**Figure 3A**); turn structure were similar with 24.23% ± 2.036% and 24.25% ± 2.472% for FGF5-WT and FGF5-Y174H, respectively (**Figure 3B**), and coil structure

was increased from 23.20% ± 3.665% to 25.98% ± 3.765% (for FGF5-WT and FGF5-Y174H, respectively) (**Figure 3C**). Secondary structures were also presented with time series graphs (**Figure 3D** and **3E**). From the 260th ns and beyond, turn and sheet structures at residues 146 to 152 (**Figure 3D**) transformed into coil structure due to the mutation (**Figure 3E**), or from the 170th ns and beyond, between residues 160 to 171, sheet structure was decreased with an increase in coil structure.

3. Decreased interaction of residue 174 with other residues is observed for Y174H

Interactions of both wild type (Y174) and mutated (H174) residues at position 174 with other residues were evaluated (**Figure 4**). Both were able to form interactions with the following residues: 91, 123, 131, 133, 162, 164, 172, 190, and 215, with the exception that the mutated Y174H residue can form a hydrogen bond with residue 163 (**Figure 4A** and **4B**). However, there was a decrease in interacting time for all the common residues for H174 and the hydrogen bond between Y174H and 163 was short-lived, as it lasted only between the initiation of the stimulation up to approximately 370th ns of the simulation (**Figure 4**). In addition, most interactions with other residues for Y174 were sustained throughout the simulations, whereas residues 131, 133, 162, 164, and 190 were sporadically sustained.

4. FGF5-Y174H experienced more movement, instability, conformational changes

To compare the movement, stability, and conformations between the wild-type and mutated proteins, data regarding C-alpha backbone RMSD, number of salt-bridges, residue RMSF (**Figure 5A**) and 2d projection of C-alpha backbone were evaluated. FGF5-Y174H with 1.677 ± 0.3614 Å demonstrated more conformational changes as well as movement throughout the simulations than FGF5-WT with 1.178 ± 0.1710 Å (**Figure 5A**). Nevertheless, RMSD values

smaller than 2 Å indicated that the starting structures were well predicted and validly constructed. At around 500th ns of the simulation FGF5-WT C-alpha RMSD was consistent most of the time with only a small spike, whereas FGF5-Y174H experienced a gradual increase in RMSD (**Figure 5A**). Inversely correlated with this trend, FGF5-WT had 60.75 ± 0.9494 salt bridges, higher than FGF5-Y174H with 5.312 ± 1.058 salt bridges, and a decrease in the number of salt-bridges could also be observed at around the 500th ns (**Figure 5B**). Additionally, the RMSF for FGF5-Y174H with 1.190 ± 0.6810 Å was higher than that of FGF5-WT 1.424 ± 0.8517 Å (**Figure 5C**). Specifically, the 3 regions with the most apparent increases for FGF5-Y174H include: residues 143 to 152, 162 to 175, and 196 to 213 (**Figure 5C**). These findings were also further examined and validated with the 2D projection of the movement of C-alpha backbone, demonstrating that the conformational movement of FGF5-Y174H was more scattered and occupied more space than FGF5-WT (**Figure 6**). In the eigenvector plot (**Figure 6**), PC1 and PC2 of FGF5-Y174 (with 0.63 and 0.322 nm², respectively) were higher than those of FGF5-WT (with 0.275 and 0.1080 nm², respectively), confirming that there was more intra-variability in the movement of C-alpha backbone for FGF5-Y174H than that of FGF5-WT.

5. The mutation increased binding affinities towards FGFR1 with altered binding mode

Binding affinities towards FGFR1, the main receptor FGF5 in regulating hair growth, was evaluated through protein-protein docking and residue interacting networking analysis (**Figure 6**). FGF5-Y174H showed a higher binding affinity towards FGFR1 than FGF5-WT (**Figure 7A** and **Figure 7C**). Residue interacting network also showed that there were 18 residues directly involved in the binding of FGF5-WT to FGFR1 (**Figure 7D**); meanwhile, the binding of FGF5-Y174H to FGFR1 had 15 residues directly involved (**Figure 7E**). Interestingly, the distribution of degree (total of connections or edges of every node or residue) was also

different (**Figure 7E**). Precisely, FGF5-Y174H had a peak at 2 degrees, whereas FGF5-WT had a peak at 1 degree and a hump at 4 degrees.

Discussion

The analysis of the molecular dynamics simulations confirmed the hypothesis that the missense mutation Y174H of FGF5 will contribute to changes in protein behaviors and structures. Particularly, interactions with the solvent, secondary structures, conformational stability, as well as connectivity with its primary receptor FGFR1 were evaluated. The mutation resulted in an increase in SASA (a biophysical marker for pathogenic protein (Savojardo et al., 2020)), further reinforced a decrease in number of hydrogen bonds within the protein and an increase in number of hydrogen bonds between the protein and solvent. Furthermore, the mutation saw a decrease in sheet but an increase in coil structures. Specifically, secondary changes were highly observable at residues 146 to 152 as well as 160 to 171. Interestingly, these residues are also in proximity with residues 91, 123, 131, 133, 162, 164, 172, 190, and 215 where H174 showed decreased and sporadic interactions compared to Y174, confirming the importance of this residue, conserved throughout multiple species (Higgins et al., 2014). Besides, analyses of the C-alpha backbone RMSD, the number of salt-bridges, and protein residue RMSF demonstrated that: compared to its wild-type counterpart, FGF5-Y174H experienced more movement, conformational changes, and fluctuations – accompanied by a decrease in the number salt-bridges, an indicator of structural stability (Bosshard et al., 2004). Lastly, we employed protein-protein docking to explore the effect of this mutation on FGFR1 binding. Contrary to our initial prediction that the missense mutation would lead to unstable binding, FGF5-Y174H demonstrated a stronger binding affinity towards FGFR1 with 15 residues directly involved than FGF5-WT with 18 residues. However, it could be speculated that FGF5-Y174H previously

demonstrated a decreased inhibition on FGFR1 (Higgins et al., 2014) because of its difference in residue signaling and connectivity. To the best of our knowledge, this is the first study to directly investigate the structure and dynamics of FGF5 as well as its missense mutation variant FGF5-Y174H, underlying trichomegaly. It is recommended that further *in vitro* and biophysical methods to validate these findings.

Funding: this study receives no funding.

Competing Interests: the author declares no competing financial interests.

References

Allerstorfer, S., Sonvilla, G., Fischer, H., Spiegl-Kreinecker, S., Gauglhofer, C., Setinek, U., Czech, T., Marosi, C., Buchroithner, J., Pichler, J., Silye, R., Mohr, T., Holzmann, K., Grasl-Kraupp, B., Marian, B., Grusch, M., Fischer, J., Micksche, M., & Berger, W. (2008). FGF5 as an oncogenic factor in human glioblastoma multiforme: Autocrine and paracrine activities. *Oncogene*, *27*(30), 4180–4190. https://doi.org/10.1038/onc.2008.61

Bosshard, H. R., Marti, D. N., & Jelesarov, I. (2004). Protein stabilization by salt bridges: Concepts, experimental approaches and clarification of some misunderstandings. *Journal of Molecular Recognition: JMR*, *17*(1), 1–16. https://doi.org/10.1002/jmr.657

Chen, B., Hu, R., Min, Q., Li, Y., Parkinson, D. B., & Dun, X.-P. (2020). FGF5 Regulates Schwann Cell Migration and Adhesion. *Frontiers in Cellular Neuroscience*, *14*, 237. https://doi.org/10.3389/fncel.2020.00237

Clementel, D., Del Conte, A., Monzon, A. M., Camagni, G. F., Minervini, G., Piovesan, D., & Tosatto, S. C. E. (2022). RING 3.0: Fast generation of probabilistic residue interaction

networks from structural ensembles. *Nucleic Acids Research*, *50*(W1), W651–W656. https://doi.org/10.1093/nar/gkac365

Han, D., Wang, M., Yu, Z., Yin, L., Liu, C., Wang, J., Liu, Y., Jiang, S., Ren, Z., & Yin, J. (2019). FGF5 promotes osteosarcoma cells proliferation via activating MAPK signaling pathway. *Cancer Management and Research*, *11*, 6457–6466. https://doi.org/10.2147/CMAR.S200234

Higgins, C. A., Petukhova, L., Harel, S., Ho, Y. Y., Drill, E., Shapiro, L., Wajid, M., & Christiano, A. M. (2014). FGF5 is a crucial regulator of hair length in humans. *Proceedings of the National Academy of Sciences of the United States of America*, *111*(29), 10648–10653. https://doi.org/10.1073/pnas.1402862111

Iwabu, J., Yamashita, S., Takeshima, H., Kishino, T., Takahashi, T., Oda, I., Koyanagi, K., Igaki, H., Tachimori, Y., Daiko, H., Nakazato, H., Nishiyama, K., Lee, Y.-C., Hanazaki, K., & Ushijima, T. (2019). FGF5 methylation is a sensitivity marker of esophageal squamous cell carcinoma to definitive chemoradiotherapy. *Scientific Reports*, *9*(1), 13347. https://doi.org/10.1038/s41598-019-50005-6

Land, H., & Humble, M. S. (2018). YASARA: a tool to obtain structural guidance in biocatalytic investigations. In *Protein Engineering* (pp. 43–67). Springer.

Li, W.-R., Liu, C.-X., Zhang, X.-M., Chen, L., Peng, X.-R., He, S.-G., Lin, J.-P., Han, B., Wang, L.-Q., Huang, J.-C., & Liu, M.-J. (2017). CRISPR/Cas9-mediated loss of FGF5 function increases wool staple length in sheep. *The FEBS Journal*, *284*(17), 2764–2773. https://doi.org/10.1111/febs.14144

Ornitz, D. M., & Itoh, N. (2015). The Fibroblast Growth Factor signaling pathway. *Wiley Interdisciplinary Reviews. Developmental Biology*, *4*(3), 215–266. https://doi.org/10.1002/wdev.176

Punzalan, F. E. R., Cutiongco-de la Paz, E. M. C., Nevado, J. J. B., Magno, J. D. A., Ona, D. I. D., Aman, A. Y. C. L., Tiongson, M. D. A., Llanes, E. J. B., Reganit, P. F. M., Tiongco, R. H. P., Santos, L. E. G., Aherrera, J. A. M., Abrahan, L. L., Agustin, C. F., Bejarin, A. J. P., & Sy, R. G. (2022). The rs1458038 variant near FGF5 is associated with poor response to calcium channel blockers among Filipinos. *Medicine*, *101*(5), e28703. https://doi.org/10.1097/MD.0000000000028703

Ren, Y., Jiao, X., & Zhang, L. (2018). Expression level of fibroblast growth factor 5 (FGF5) in the peripheral blood of primary hypertension and its clinical significance. *Saudi Journal of Biological Sciences*, *25*(3), 469–473. https://doi.org/10.1016/j.sjbs.2017.11.043

Rossetto, J. D., Nascimento, H., Muccioli, C., & Belfort, R. (2013). Essential trichomegaly: Case report. *Arquivos Brasileiros De Oftalmologia*, *76*(1), 50–51. https://doi.org/10.1590/s0004-27492013000100015

Savojardo, C., Manfredi, M., Martelli, P. L., & Casadio, R. (2020). Solvent Accessibility of Residues Undergoing Pathogenic Variations in Humans: From Protein Structures to Protein Sequences. *Frontiers in Molecular Biosciences*, *7*, 626363. https://doi.org/10.3389/fmolb.2020.626363

Xin, Q., Han, Y., Jiang, W., Wang, J., Luan, Y., Ji, Q., & Sun, W. (2022). Genetic susceptibility analysis of FGF5 polymorphism to preeclampsia in Chinese Han population. *Molecular Genetics and Genomics: MGG*, *297*(3), 791–800. https://doi.org/10.1007/s00438-022-01889-z

Xue, L. C., Rodrigues, J. P., Kastritis, P. L., Bonvin, A. M., & Vangone, A. (2016). PRODIGY: A web server for predicting the binding affinity of protein–protein complexes. *Bioinformatics*, btw514. https://doi.org/10.1093/bioinformatics/btw514

Yan, Y., Zhang, D., Zhou, P., Li, B., & Huang, S.-Y. (2017). HDOCK: A web server for protein-protein and protein-DNA/RNA docking based on a hybrid strategy. *Nucleic Acids Research*, *45*(W1), W365–W373. https://doi.org/10.1093/nar/gkx407

Figure Captions

Figure 1. Ramachandran plots validating the structures of FGF5-WT and FGF5-Y174H. Both plots demonstrate that both proteins are energetically preferred with 130 (97.015%) highly preferred, 4 (2.985%) preferred, and no questionable observations.

Figure 2. Behavioral parameters of wild-type fibroblast growth factor 5 (FGF5-WT) and its Y174H missense mutation variant (FGF5-Y174H). (A) Solvent accessible surface areas (SASA) in $Å^2$ over 1,000 ns. (B) Number of hydrogen bonds within the proteins. (C) Number of hydrogen bonds between the protein and solvent

Figure 3. Assessment of secondary structure assessment over time. Violin graphs depicting the distributions of (A) sheet (B) turn (C) coil secondary structures over time. Color-filled time-series graphs depicting the evolutions of these structures over time for (D) FGF5-WT and (E) FGF5-Y174H.

Figure 4. Analyses of interactions of Y174 and H174 with other residues. Bar graphs depicting the accumulations of interactions of residue 174 with others for (A) the wild-type Y174 and (B) the missense mutation variant H174. Color-filled time-series graphs depicting the

evolutions of these interactions over time for (C) Y174 and (D) H174; white space denotes no interaction.

Figure 5. Stability and conformation parameters of FGF5-WT and FGF5-Y174H. (A) Root mean-square deviation (RMSD) of C-alpha backbones. (B) Number of salt-bridges formed by the interactions of lysine (Lys)/ arginine (Arg) with aspartic acid (Asp)/ glutamic acid (Glu). (C) Root mean-square fluctuations (RMSF).

Figure 6. Principal component analysis (PCA) for the movement of C-alpha backbone. 1,000 simulation snapshots capturing equidistance conformations were analyzed from the beginning to end of simulations. The first two eigenvectors were retrieved and visualized on 2D graph.

Figure 7. Protein-protein docking and residue interacting network analysis. Visualizations of docked protein-protein complexes with binding affinities (ΔG, in kcal/mol) for (A) FGF5-WT-FGFR1 and (C) FGF5-Y174H-FGFR1. Network analysis of residue interactions for (B) FGF5-WT-FGFR1 and (C) FGF5-Y174H-FGFR1. (D) Histogram depicting changes in the distributions of degree for FGF5-WT-FGFR1 and FGF5-Y174H-FGFR1.

FGF5-WT

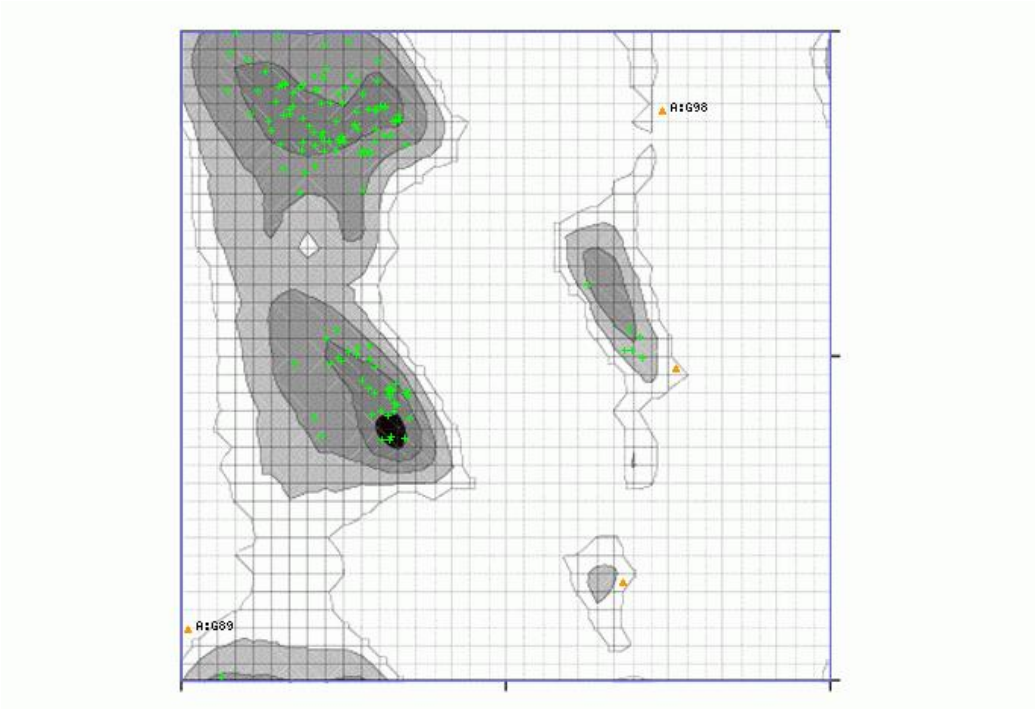

FGF5-Y174H

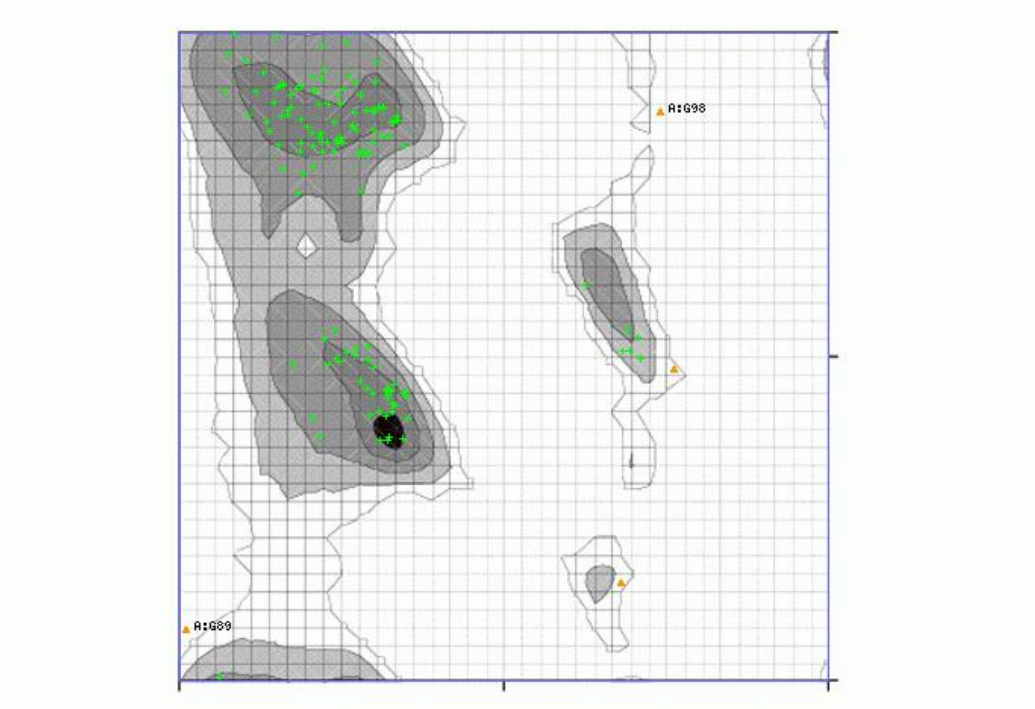

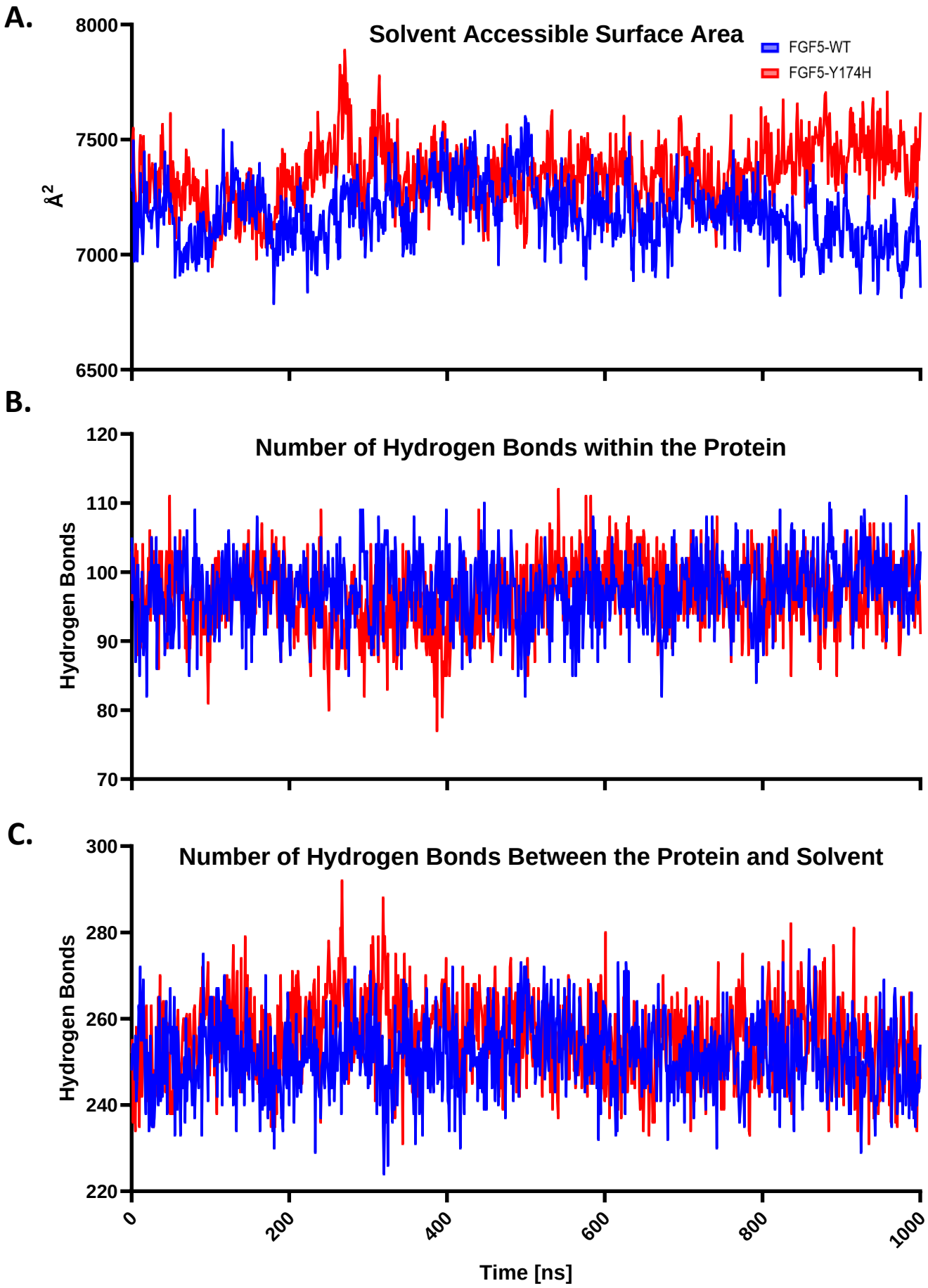
A.
Solvent Accessible Surface Area
FGF5-WT
FGF5-Y174H
Å2
8000
7500
7000
6500
B.
Number of Hydrogen Bonds within the Protein
Hydrogen Bonds
120
110
100
90
80
70
C.
Number of Hydrogen Bonds Between the Protein and Solvent
Hydrogen Bonds
300
280
260
240
220
0
200
400
600
800
1000
Time [ns]

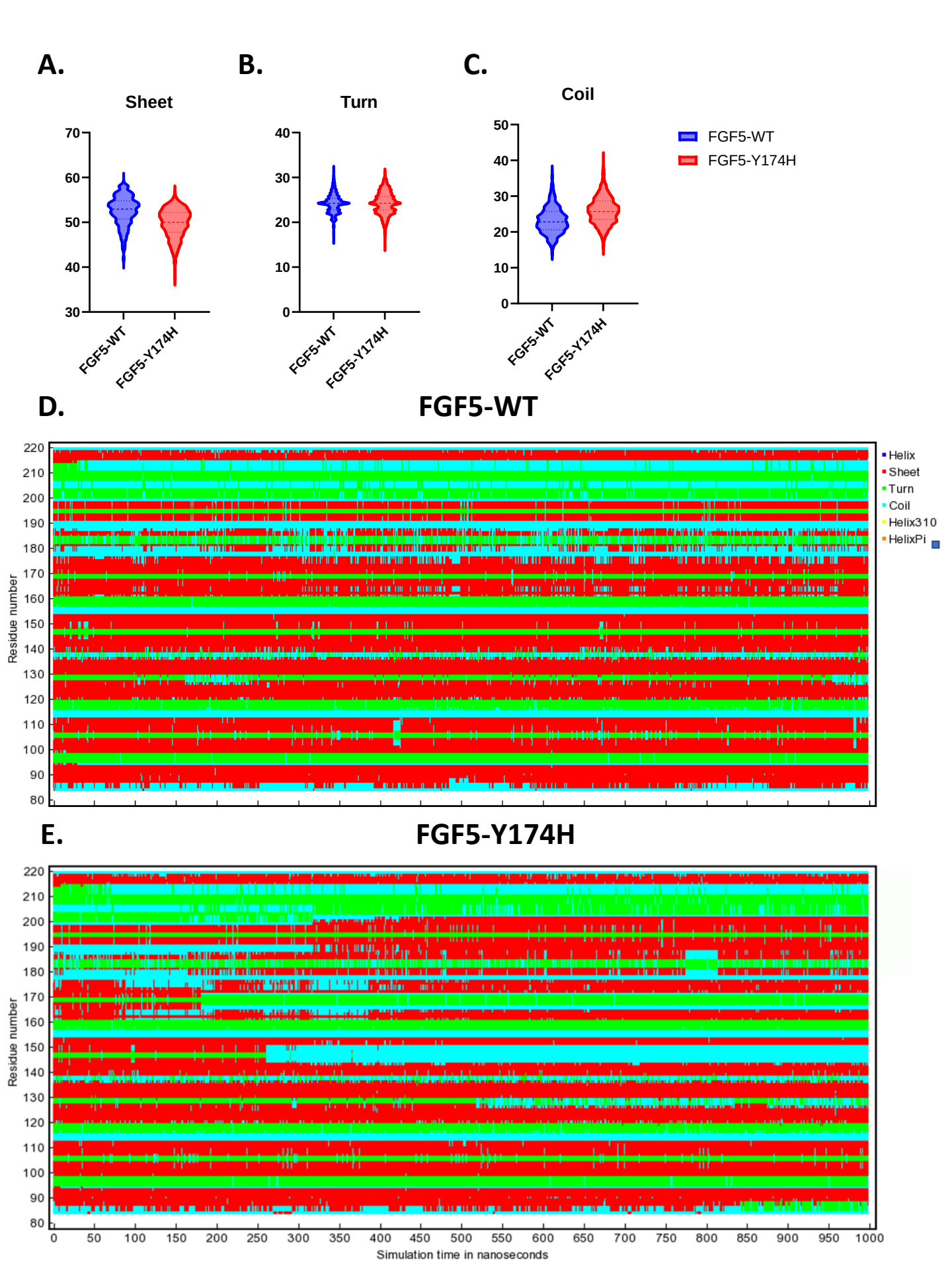
A.
Sheet
70
60
50
40
30
FGF5-WT
FGF5-Y174H
B.
Turn
40
30
20
10
0
FGF5-WT
FGF5-Y174H
C.
Coil
50
40
30
20
10
0
FGF5-WT
FGF5-Y174H
FGF5-WT
FGF5-Y174H
D.
FGF5-WT
Residue number
220
210
200
190
180
170
160
150
140
130
120
110
100
90
80
Helix
Sheet
Turn
Coil
Helix310
HelixPi
E.
FGF5-Y174H
Residue number
220
210
200
190
180
170
160
150
140
130
120
110
100
90
80
0
50
100
150
200
250
300
350
400
450
500
550
600
650
700
750
800
850
900
950
1000
Simulation time in nanoseconds

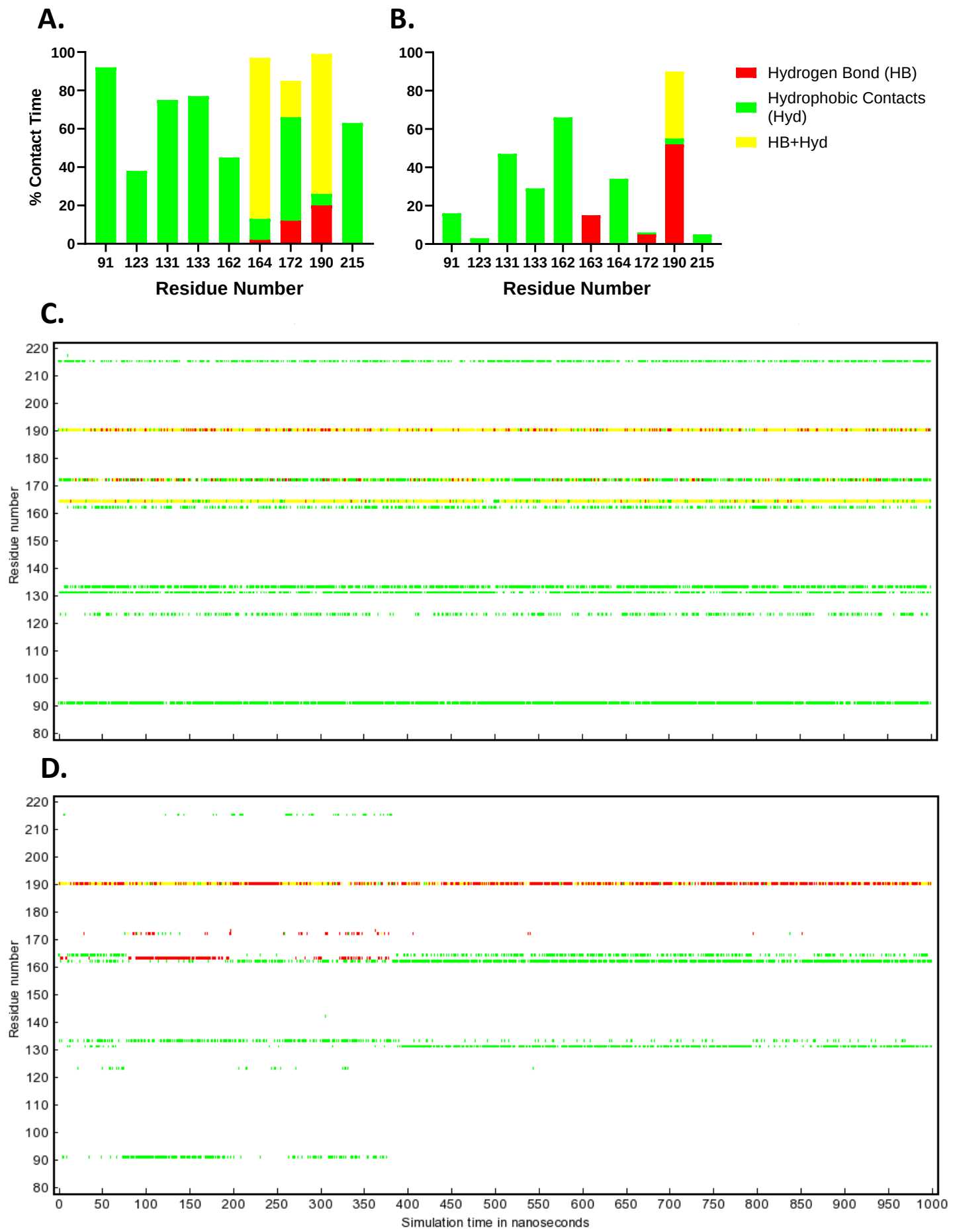
A.
% Contact Time
100
80
60
40
20
0
91 123 131 133 162 164 172 190 215
Residue Number
B.
100
80
60
40
20
0
91 123 131 133 162 163 164 172 190 215
Residue Number
Hydrogen Bond (HB)
Hydrophobic Contacts (Hyd)
HB+Hyd
C.
Residue number
220 210 200 190 180 170 160 150 140 130 120 110 100 90 80
D.
Residue number
220 210 200 190 180 170 160 150 140 130 120 110 100 90 80
0 50 100 150 200 250 300 350 400 450 500 550 600 650 700 750 800 850 900 950 1000
Simulation time in nanoseconds

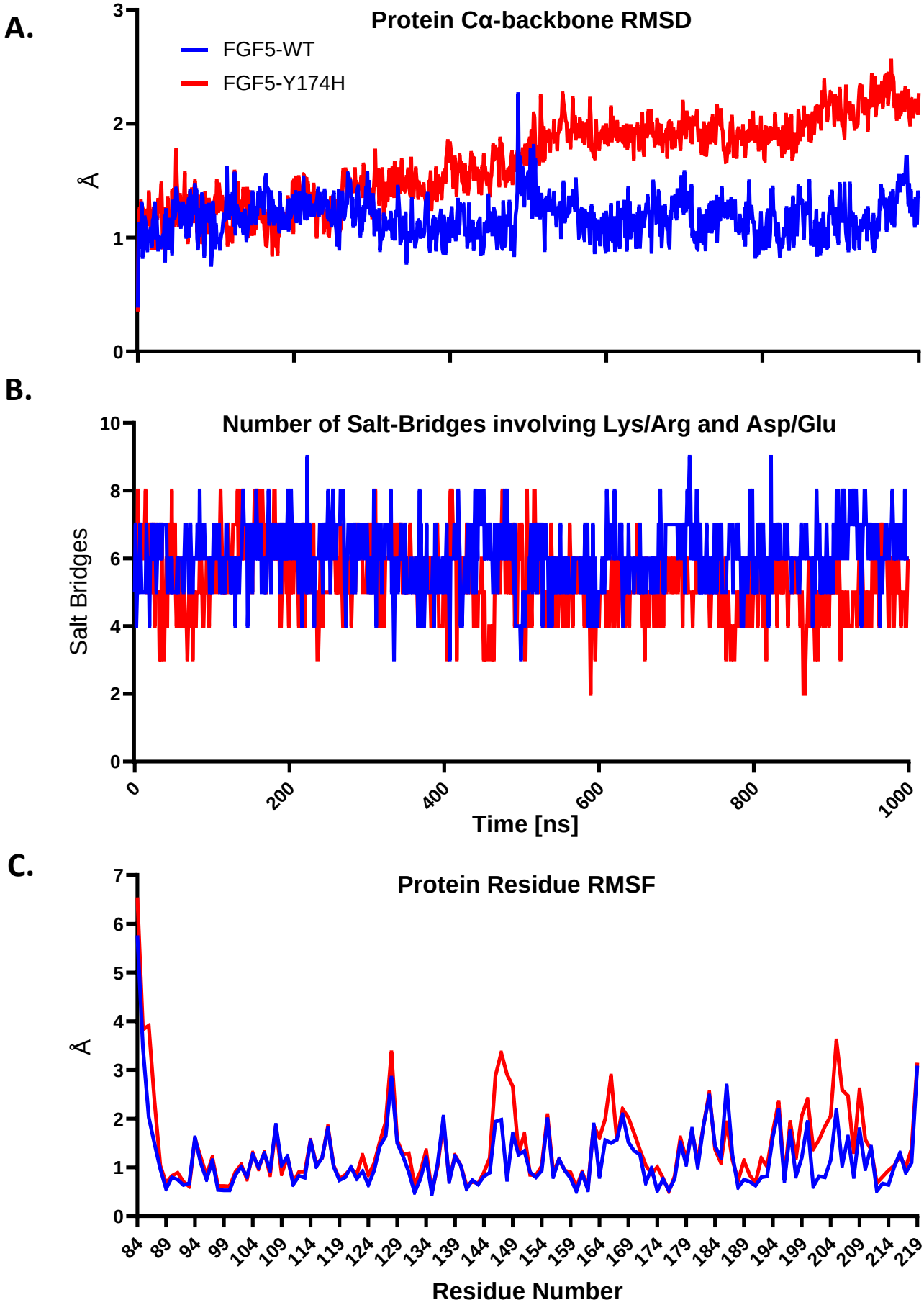
A.
Protein Cα-backbone RMSD
FGF5-WT
FGF5-Y174H
Å
0
1
2
3
B.
Number of Salt-Bridges involving Lys/Arg and Asp/Glu
Salt Bridges
0
2
4
6
8
10
0
200
400
600
800
1000
Time [ns]
C.
Protein Residue RMSF
Å
0
1
2
3
4
5
6
7
84
89
94
99
104
109
114
119
124
129
134
139
144
149
154
159
164
169
174
179
184
189
194
199
204
209
214
219
Residue Number

2D Projection of trajectory

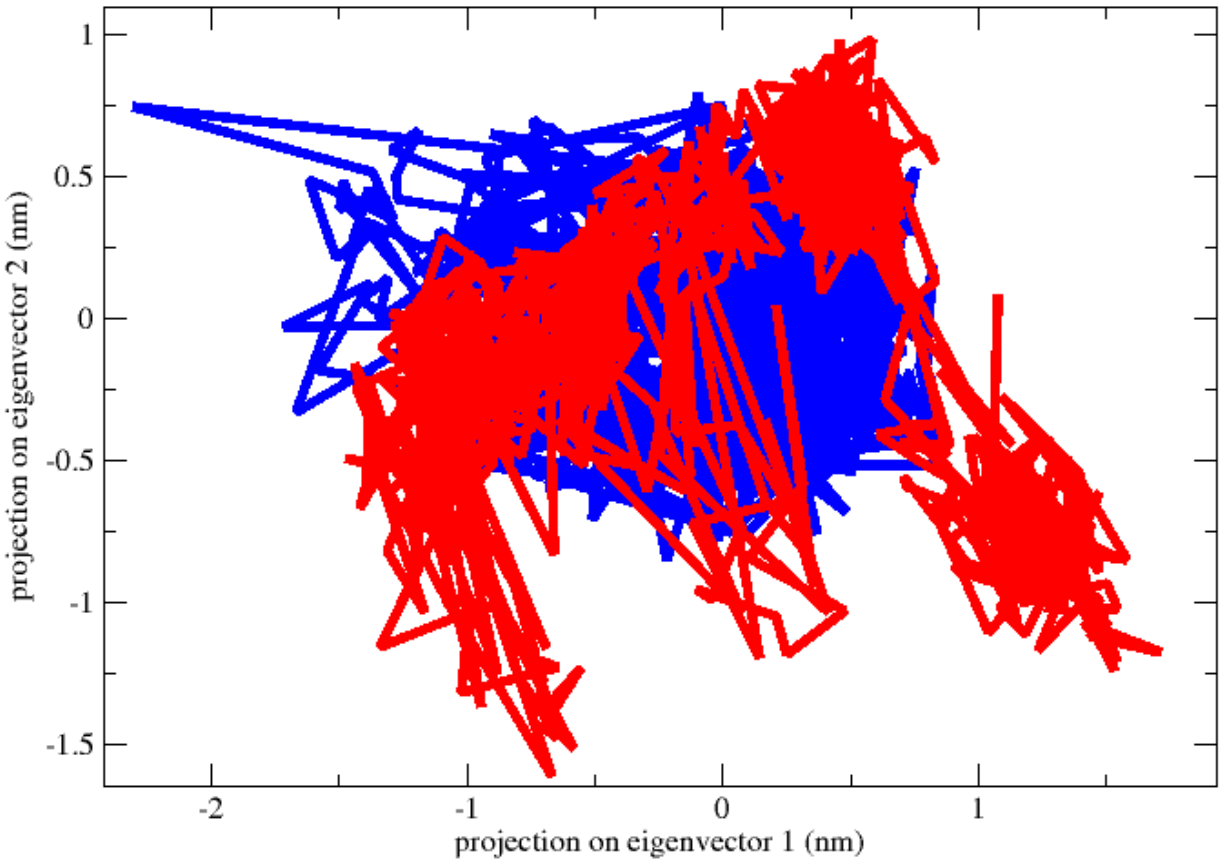

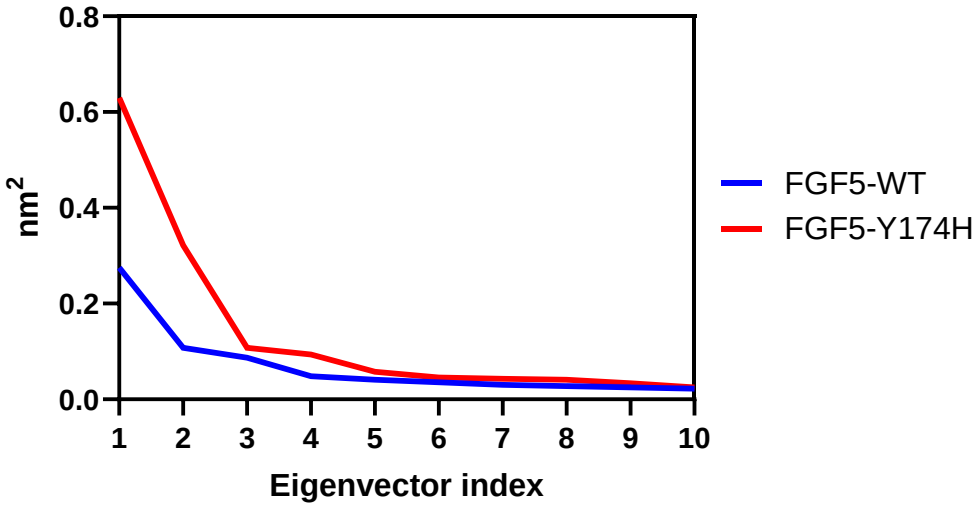

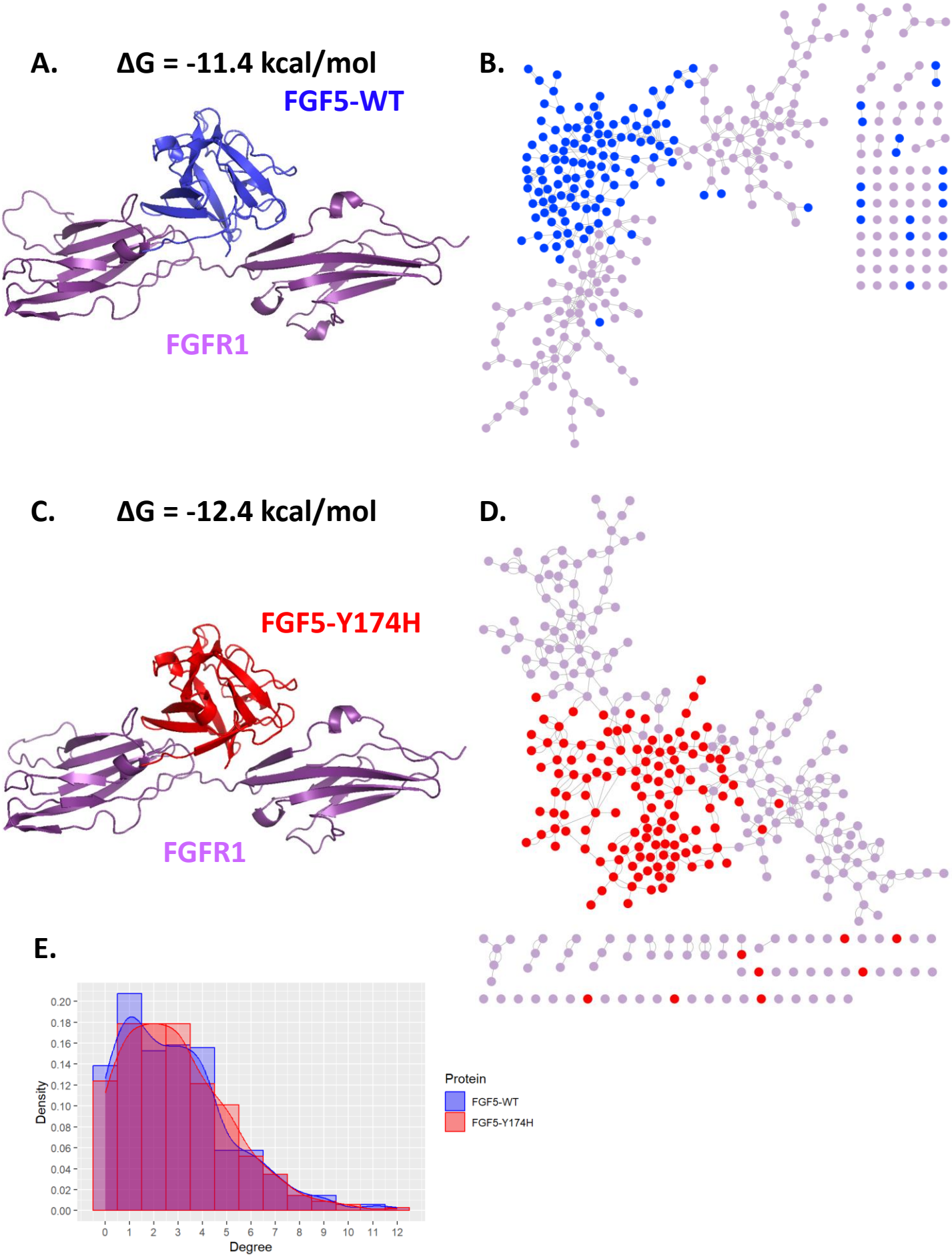
A.
ΔG = -11.4 kcal/mol
FGF5-WT
FGFR1
B.
C.
ΔG = -12.4 kcal/mol
FGF5-Y174H
FGFR1
D.
E.
Density
Degree
Protein
FGF5-WT
FGF5-Y174H